TREASURES @UT Dallas

UT DALLAS | Eugene McDermott Library

Erik Jonsson School of Engineering and Computer Science

2013-10-17

Electrical Design of InAs-Sb/GaSb Superlattices for Optical Detectors using Full Bandstructure Sp^3s^* Tight-Binding Method and Bloch Boundary Conditions

UTD AUTHOR(S): Raja Mir and William R. Frensley

©2013 AIP Publishing LLC

Find more research and scholarship conducted by the Erik Jonsson School of Engineering and Computer Science here. This document has been made available for free and open access by the Eugene McDermott Library. Contact libwebhelp@utdallas.edu for further information.

JOURNAL OF APPLIED PHYSICS **114**, 153706 (2013)

Electrical design of InAs-Sb/GaSb superlattices for optical detectors using full bandstructure sp^3s^* tight-binding method and Bloch boundary conditions

Raja N. Mir[a)] and William R. Frensley[b)]
Erik Jonsson School of Engineering and Computer Science, The University of Texas at Dallas, Richardson, Texas 75083, USA

(Received 2 May 2013; accepted 20 September 2013; published online 17 October 2013)

InAs-Sb/GaSb type-II strain compensated superlattices (SLS) are currently being used in mid-wave and long-wave infrared photodetectors. The electronic bandstructure of InSb and GaSb shows very strong anisotropy and non-parabolicity close to the Γ-point for the conduction band (CB) minimum and the valence band (VB) maximum. Particularly around the energy range of 45–80 meV from band-edge we observe strong non-parabolicity in the CB and light hole VB. The band-edge dispersion determines the electrical properties of a material. When the bulk materials are combined to form a superlattice we need a model of bandstructure which takes into account the full bandstructure details of the constituents and also the strong interaction between the conduction band of InAs and valence bands of GaSb. There can also be contact potentials near the interface between two dissimilar superlattices which will not be captured unless a full bandstructure calculation is done. In this study, we have done a calculation using second nearest neighbor tight binding model in order to accurately reproduce the effective masses. The calculation of mini-band structure is done by finding the wavefunctions within one SL period subject to Bloch boundary conditions $\psi(L) = \psi(0)e^{ikL}$. We demonstrate in this paper how a calculation of carrier concentration as a function of the position of the Fermi level (E_F) within bandgap(E_g) should be done in order to take into account the full bandstructure of broken-bandgap material systems. This calculation is key for determining electron transport particularly when we have an interface between two dissimilar superlattices. © *2013 AIP Publishing LLC*. [http://dx.doi.org/10.1063/1.4824365]

I. INTRODUCTION

The InAs-Sb/GaSb type-II SLS[1] are being examined for the realization of high-performance infrared detectors.[2] They offer a number of advantages over HgCdTe like large effective mass which reduces tunneling,[1,3] reduction in auger recombination process,[4] E_g tunability and uniformity. The performance of these detectors is directly related to the fundamental carrier transport physics. The electrical properties of InAs-Sb/GaSb SLS are determined by the carrier distribution close to the band edges of the fundamental E_g.

In past type-II SLS have been analyzed[5] using the empirical tight binding method. In this study nearest neighbour Hamiltonian with two-center approximation was used. A good agreement of E_g between theory and experiment was obtained but the dispersion over the entire Brillion zone was not evaluated, they have only calculated E_g, i.e., bandstructure at $k = 0$ and other essential quantities for the electrical design of the device like density of states (DOS) and carrier concentrations with respect to position of E_F in the E_g have not been calculated. Electronic structure of this material system has also been calculated using effective mass theory[6] about the Γ-point. The effective mass approach will not take into account the non-parabolic nature of the energy bands near the band edges which is critically important to determine the DOS with greater precision. The InAs-InSb/GaSb systems are broken gap. Hence, there is interaction between the CB of InAs and the VB's of InSb/GaSb at a very high value of the energy from the InAs valence band edge, therefore, we need a model of bandstructure which accounts for the details of bandstructure close to as well as far from the bandedge, in other words, we need a full bandstructure model to capture all the interactions. The $\mathbf{k} \cdot \mathbf{p}$ approach[7] for bandstructure calculation of these systems is also being used and we can take the non-parabolicity of the bandstructure into account.[8] But it still suffers from two main drawbacks one is that with this method the non-isotropic nature of energy bands about the energy axis near the band edges cannot be taken into account, second the basis in $\mathbf{k} \cdot \mathbf{p}$ is not localized which makes a technique like tight binding with localized basis where the wavefunction of carriers is resolved to the extent of atomic spacing a better choice since these SLS are grown epitaxially.

Empirical tight binding method since its beginning[9] has evolved[10,11] and has been widely used to model III–V's and silicon.[12–17] We have used the second nearest neighbour[18] sp^3s^* empirical tight binding model(SNTB) with spin-orbit coupling in this paper to model type-II SL without doing the two centre approximation. The energy gaps both direct and indirect, Γ and X valley effective masses are fit closely. In this paper, we do a comprehensive analysis of the complementary barrier infrared detector(CBIRD) detector[2] using our bandstructure model with Bloch type of boundary

a)Electronic mail: rnm063000@utdallas.edu
b)Electronic mail: frensley@utdallas.edu

 © 2013 AIP Publishing LLC

conditions on the absorber and the electron barrier superlattice. We obtain from our calculations the energy bandstructure, DOS, electron and hole wavefunction in a unit cell of a broken gap superlattice and carrier concentrations. Accurate knowledge of these quantities is essential for simulations of electronic transport.

The CBIRD infrared detector uses type-II InAs/GaSb SL for detection of the infrared radiation. Design of CBIRD consists of 600 period absorber SL (44 Å,21Å) InAs,GaSb sandwiched between an 80 period of hole barrier SL (46 Å,12Å) InAs,AlSb and 60 period electron barrier SL (22 Å,21Å) InAs,GaSb. Fig. 1 shows the electron/hole barrier SL unit cells. The hole barrier SL and the electron barrier SL are designed to have zero conduction and valence subband offset with respect to the absorber SL. The materials InAs, InSb, and GaSb belong to the category of 6.1 Å material system and are nearly lattice matched. InAs has the bandgap of 0.36 eV, GaSb has the bandgap of 0.78 eV and the offset between the valence bands of two materials is 0.51 eV this leads to the type II or the broken gap alignment which in turn results in the overall bandgap of the material system to be useful for infrared detection and also tunable by changing the ratio of the InAs to GaSb layers. In between InAs and the GaSb layers in the absorber, a monolayer of InSb is used for strain compensation. At present CBIRD structures are being nominally doped[2] and there is no clear understanding of how E_F will vary with doping in these structures. In this paper, we will analyze the CBIRD so that have a sound theoretical handle on the electrical design of these structures.

Conceptually, a CBIRD detector could be made from uniform semiconductor alloys, rather than SLS. But since SLS can be grown with better control and reproducibility than a uniform alloy they are grown epitaxially. The fabricated devices appear to have more of an energy barrier than is expected.[19] We conjecture that this barrier may be due not to the well-studied flat-band heterojunction alignment, but due to a contact-potential induced band bending near the heterojunction. Such a contact potential is produced when the equilibrium E_F's do not align in the flat-band condition and should be removable by a judicious choice of doping densities. But in order to choose a proper doping level, we need to know the density of states distribution in the superlattice.

II. METHOD

A. Superlattice bandstructure

In the tight binding basis, we can model III–V compounds by alternating sets of planar orbitals of anions and cations along the direction of growth in 001-direction of a thick SL. A layer is formed by two planar orbitals of anions and cations and occupies a space of $a/2$ along 001 direction. In the second nearest neighbor model, each atomic plane is coupled to two previous and two next adjoining atomic planes.

The SL bandstructure is computed by solving the following eigenvalue problem:

$$H_{Superlattice}\psi + I\mathbb{E}_{\mathbf{off}} = E\psi, \tag{1}$$

where E is the energy, ψ is the wavevector whose dimensions are $(20N_{SL})\times 1$ where: N_{SL} is the number of layers of the superlattice. In each 20×1 block if the first 10×1 correspond to the anion then first half 5×1 correspond to one spin and the other half to the other spin and similarly for the cation. $\mathbb{E}_{\mathbf{off}}$ is the bandoffset. The band offset data, $\mathbb{E}_{\mathbf{off}}$ given[21] cannot be directly used directly since we need to incorporate the effect of the spin orbit splitting which changes the offsets in the model. The band offsets given in Table I have been used using InAs as the reference at 0 eV.

The overall superlattice Hamiltonian is given by

$$H_{Superlattice} = \begin{bmatrix} D_{Self}^{1,1} & S_{Next}^{1,2} & 0 & 0 & 0 & \dots & e^{ik_zL}S_{Next}^{n,1} \\ S_{Previous}^{1,2} & D_{Self}^{2,2} & S_{Next}^{2,3} & 0 & 0 & \dots & 0 \\ 0 & S_{Previous}^{2,3} & D_{Self}^{3,3} & S_{Next}^{3,4} & 0 & \dots & 0 \\ 0 & 0 & S_{Previous}^{3,4} & D_{Self}^{4,4} & S_{Next}^{4,5} & \dots & 0 \\ \vdots & \vdots & \vdots & \ddots & \ddots & \ddots & \vdots \\ 0 & 0 & 0 & \dots & S_{Previous}^{n-2,n-1} & D_{Self}^{n-1,n-1} & S_{Next}^{n-1,n} \\ e^{-ik_zL}S_{Previous}^{1,n} & 0 & 0 & \dots & 0 & S_{Previous}^{n,n-1} & D_{Self}^{n,n} \end{bmatrix}. \tag{2}$$

D_{Self} corresponds to the intralayer coupling within the same layer as well as interlayer couplings with adjoining layers as well. $S_{Previous}$ and S_{Next} corresponding to the previous and next interlayer couplings, respectively. The dimension for each of $S_{Previous}$, D_{Self} and S_{Next} matrices is 20×20. These matrices are constructed using the submatrices and parameters provided by Boykin.[18,20] On the top right corner and the bottom left corners, we use $S_{Next}e^{ik_zL}$ and $S_{Previous}e^{-ik_zL}$, L being the length of the superlattice. These are the Bloch boundary conditions. The boundary conditions capture the fact that the wavefunction is periodic $\psi(L) = \psi(0)e^{ikL}$ or the superlattice unit cell is repeated.

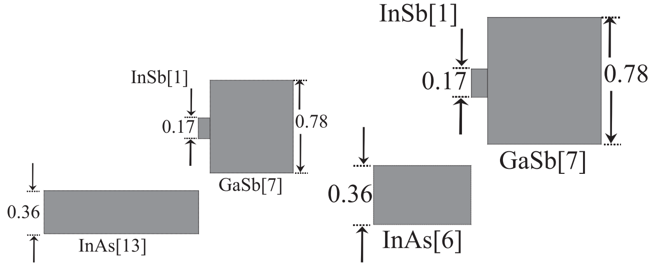

FIG. 1. The unit cells of the CBIRD absorber on the left and that of the electron barrier on the right. The grey area represents E_g in eV's. The numbers next to the compound names in square brackets are the number of layers. The electron barrier has less number of InAs layers as compared to the absorber which makes its E_g wider. The number of GaSb layers is same in both absorber and the electron barrier SLS. Both SLS have an extra layer of InSb in the middle which is there for strain compensation.

Once the bandstructure is obtained by solving the eigenvalue problem. The fundamental E_g is found by finding the energies at $k=0$ and sorting them in ascending order and finding the $2/5th$ element of the sorted data set which corresponds to the top of VB edge.

The E_g can vary with temperature and the dependence on temperature can be modeled by following empirical dependance[22]

$$E_g(T) = E_g(0) - \frac{aT^2}{b+T}, \tag{3}$$

where experimentally determined[23] values can be used for a and b. The value of $b=270\,K$ and a will vary[23] with number of layers of the constituents. There could be another source of the change in bandstructure with temperature which is that the effective masses could change with temperature. We could not find the temperature dependence of the effective masses in the literature. These variations in E_g as a function of temperature will lead to a band edge shifting between two dissimilar superlattices even if they are designed for no barrier at a particular temperature. The band-offset can also vary with temperature.

Using the superlattice Hamiltonian the oscillator strength[24] and momentum matrix element can be easily determined. The momentum operator p can be found using

$$p = \frac{m\nabla_k H(k)}{\hbar}, \tag{4}$$

this can be used to find the momentum matrix element p_{mn} between two bands at a particular k value by using:

$$p_{mn} = \langle m|p|n\rangle. \tag{5}$$

TABLE I. Band offset data, $\mathbb{E}_{\mathbf{off}}$ (eV).

Compound	Band offset
GaSb	0.1700
InAs	−0.0100
InSb	0.4130
AlSb	0.2700
GaAs	−0.2172
AlAs	0.3000

And finally the oscillator strength f_{mn} can be found as

$$f_{mn} = \frac{2|p_{mn}|^2}{m\hbar\omega_v}, \tag{6}$$

where m is the electron mass and $\hbar\omega_v = E_{mk} - E_{nk}$, the E's being the band edges of mth and nth band at a particular k. A detailed calculation of the optical properties of these structures will be done in another publication.

B. Density of states calculation

Next, we calculate E over a $2D$ mesh of k values, E Vs (kx,kz). We are assuming that the superlattice is in z-direction [001] and the (x,y) plane is perpendicular to the direction of growth of the superlattice. The composition will vary in z direction only and not in x or y direction. In order to compute DOS, we do an axial approximation in the (k_x, k_y) plane in the k-space, we assume that the energy will be same for the circle with radius $2\pi kx$. In order to calculate the DOS, we transform the integral over wavevector(k) to energy(E). This can be done by using the following relationship:[8]

$$\int_{E_C}^{\infty} D(E)dE \leftrightarrow 2\int \frac{d^3\mathbf{k}}{(2\pi)^3}, \tag{7}$$

where D(E) will represent the density of states in $eV^-1\,nm^-3$. Equation (7) is computed by taking the bandstructure over mesh of (kx,kz) and finding the range of energy. The energy axis is then divided in to a number of intervals and corresponding to each point in a particular interval range in the energy axis we count $2\pi kx$ (axial approximation) per point and sum all the points in a particular interval. Once we have done this over the energy range. We then divide the count by dE and multiply the result by $2\frac{\mathbf{dk_x dk_z}}{(2\pi)^3}$, which gives us the DOS.

Using this we can calculate the carrier concentration's with respect to E_F position within the E_g. We can now use these arrays to represent a superlattice as an effective material for further transport simulation. Therefore, we have an accurate mapping between the position of E_F in the E_g and doping concentration.

III. RESULTS AND ANALYSIS

A. Comparison between effective mass and tight-binding bulk bandstructures and absorber/electron barrier bandstructures

In Fig. 2, we have two sets of (InAs, GaSb) plots. We are plotting the full bandstructure plots of these compounds and the effective mass plots of the CB and VB's of these compounds. Once we overlay these plots we can see that the effective mass approximation deviates from the full bandstructure. Also we can observe that there is interaction between the conduction band of InAs and the valence bands of GaSb. Therefore, we need a model which captures this interaction mathematically in form of coupling between these bands. The SNTB model captures this interaction. At

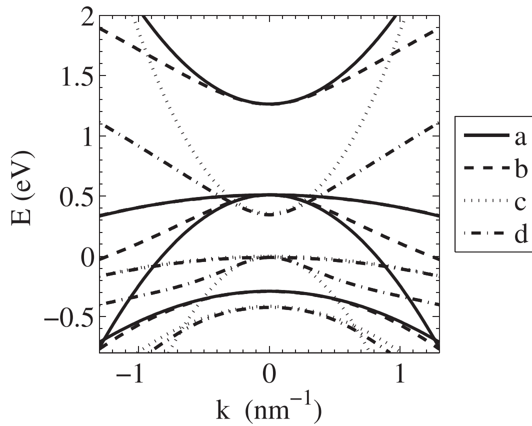

FIG. 2. The various sets of curves in the plot are: "a" refers to bandstructure of GaSb obtained using effective mass model, "b" refers to bandstructure of GaSb obtained using SNTB, "c" refers to bandstructure of InAs obtained using effective mass model and "d" refers to bandstructure of InAs obtained using SNTB. We can clearly see that the tight binding model and effective mass model would give us very different results since at the values of energy away from the bandedge the effective mass model diverges from the full bandstructure model. Also we can clearly see that there is interaction between the valence bands of GaSb and the conduction band of InAs which can be captured by the SNTB.

the energy range of 45–80 meV from bandedge we observe strong non-parabolicity in the CB and light hole VB.

The band structures of the absorber and the electron barrier are shown in Figs. 3 and 4. The Absorber Fig. 1 unit cell has more number of the InAs layers than electron barrier superlattice which leads it to have smaller bandgap. The bandgap of absorber is 0.132 eV and that of electron barrier is 0.3104 eV. The electronic bandstructures for these structures are calculated using the Hamiltonian provided in the appendix.

B. E_g variation as a function of number of layers of constituents

The dependence of the SL E_g as a function of the number of layers of InAs/GaSb layers is studied next Fig. 5; with and without a monolayer of InSb. The extra Sb layer makes a very significant difference in the E_g. We also observe that the addition of GaSb layers will increase the E_g of the system to begin with if we have 14 InAs layers but if we exceed a

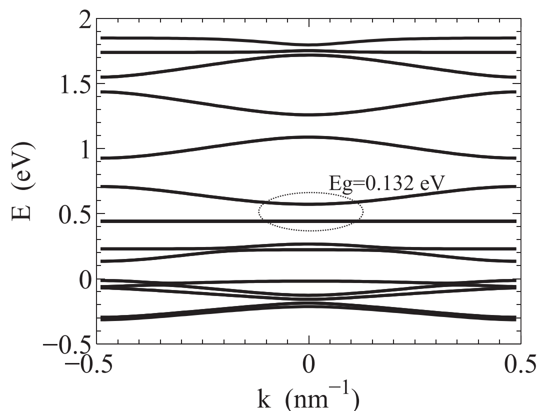

FIG. 3. The Energy Vs Wavevector relationship of absorber SL. The absorber SL has a fundamental E_g of 0.132 eV.

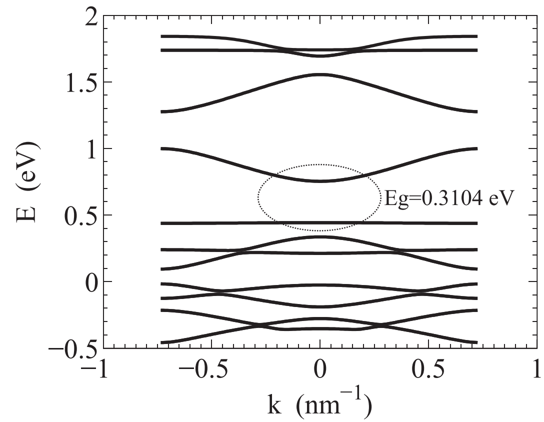

FIG. 4. The Energy Vs Wavevector relationship of electron barrier SL. The electron barrier SL has a fundamental E_g of 0.3104 eV and acts like a barrier to electrons in the absorber.

certain number of InAs layers we find that the addition of the GaSb layers will actually decrease the E_g of the overall system, this is counterintuitive since the addition of a larger E_g material should increase the E_g.

C. Electron and hole wavefunctions in a unit cell

We also looked at the electron and hole wavefunctions in Fig. 6. In the superlattice with and without InSb. We notice that the introduction of the InSb monolayer alters both the electron and the hole wavefunction, there are two structures for which we have calculated the electron and hole wavefunctions both have 22 layers. In the structure without InSb mono-layer, there are 15 InAs layers and 7 GaSb layers. In the structure with InSb mono-layer there are 14 InAs layers 1 InSb layer and 7 GaSb layers. If we look at Fig. 1, we can see that the conduction bands of InAs, InSb, and GaSb form an electron well over InAs and the valence bands form a well for holes over GaSb. In Fig. 6, we can see the impact of the InSb layer on the wavefunctions. Hole

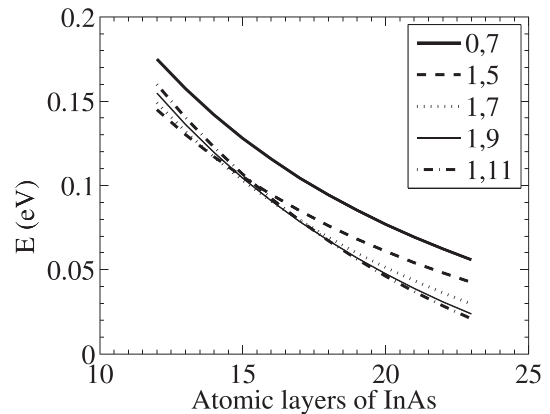

FIG. 5. Variation of the E_g with respect to the number of layers of InAs, the subscripts in the legend are (InSb layer),(GaSb layers). By adding an extra layer of InSb in the middle we see the overall E_g becomes smaller since the InSb layer in the middle has smaller E_g than either InAs or GaSb. We also see that increasing the InAs layers will reduce the E_g and increasing the GaSb layers will increase the E_g but it is predicted by our model that as we increase the number of InAs layers increasing the number of GaSb layers say at 20 InAs layers will have opposite effect, which is that it will actually decrease the bandgap.

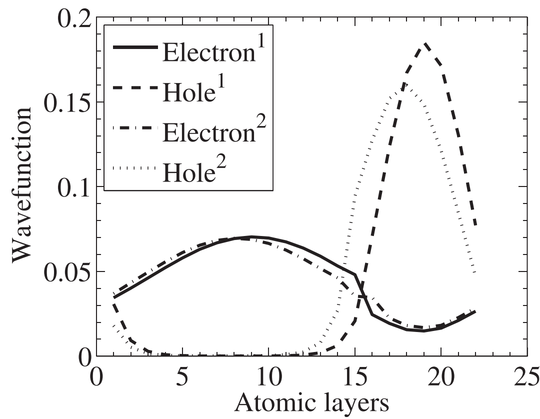

FIG. 6. The electron and hole wavefunctions within the unit cell of a superlattice. The superscripts indicate 1(without) and 2(with) the InSb monolayer. There first 15 layers are InAs and the last 7 layers are GaSb when the curves begin and then the number of InAs layers is increased as depicted in x-axis of the plot.

wavefunction drifts towards the center of the structure and electron wavefunction is not impacted much only near the center the electron wavefunction does not decay as rapidly as it had decayed before when we did not have InSb monolayer. The net overlap between the wavefunctions has increased. Intuitively this can be understood in terms of the fact that electrons behave like marbles they tend to roll down the bandstructure in real space and holes behave like bubbles and they tend to move up in the bandstructure. When we look at the bandstructure before we have added the InSb layer we see that the electron and hole are in their respective wells. After we add the extra InSb layer, we find that the holes find a taller notch to get into and hence their wavefunction moves towards the center of the structure. The electrons do not find anything like this instead the deepest the conduction band is still over InAs and since we added only a monolayer the impact on the electron wavefunction is not much.

D. DOS in absorber and electron barrier

Fig. 7 illustrates the comparison between the electron and the hole barrier DOS. We can observe that the electron barrier DOS is offset from the absorber DOS with respect to the conduction band. This is expected because the barrier is supposed to stop the flow of electrons and if there are no

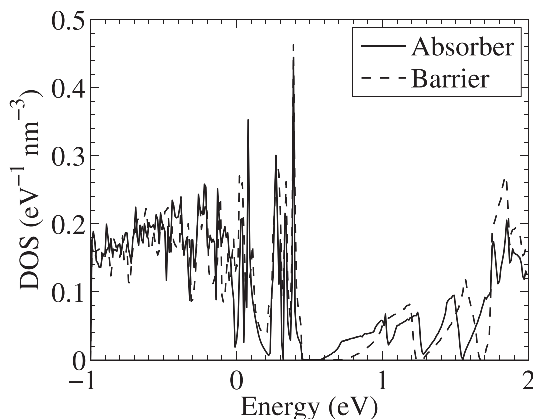

FIG. 7. Density of states comparison between absorber SL and the electron barrier SL.

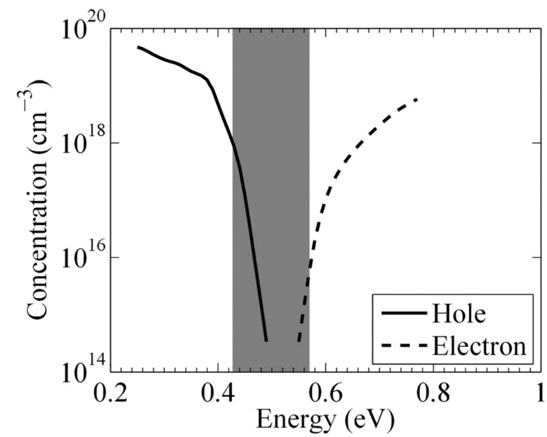

FIG. 8. The E_F position Vs electron/hole concentration of absorber SL. Dark region is the fundamental E_g.

propagating states corresponding to the Absorber conduction band states in Electron barrier the electrons will be blocked by the barrier. In case of the valence bands DOS overlap to a much greater extent. The plots of the 3D-DOS are non parabolic with respect to the DOS axis. Since the bandstructure is non-parabolic this is there in the DOS calculation as well. The DOS is more complicated in the valence band than in the conduction band because of the mini-band structure in the valence band of the superlattice bandstructures.

E. E_F position as a function of carrier concentration (doping)

Finally, we plot the electron and hole concentrations in the two SLS with respect to the position of the E_F Figs. 8 and 9. As we move close to the VB edge the hole concentration increases and the electron concentration decreases, if we move towards the CB edge the electron concentration increases and hole concentration decreases which is expected, since this information is obtained from a full bandstructure model of these materials these results are very accurate. This information can be used further to draw bandstructures in real space and calculate the position of the E_F with respect to the band-edges in the absorber and the electron barrier knowing what the dopings are in the respective regions. Once we know where the E_F is in each of the

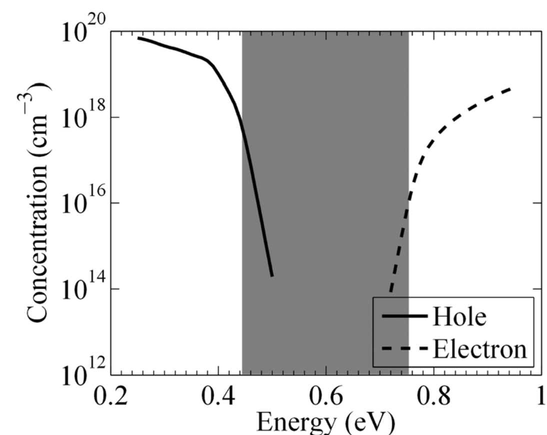

FIG. 9. The E_F position Vs electron/hole concentration of electron barrier SL. Dark region is the fundamental E_g.

materials we can then draw the energy band diagram to find out if there is a barrier between two SLS and how much do we need to dope the various regions to optimize the electrical design of the device.

IV. SUMMARY AND CONCLUSIONS

We have done a rigorous analysis of CBIRD detector which consists of InAs-InSb/GaSb type-II SL layers. We have used second nearest neighbour sp3s* tight binding model to evaluate the bandstructure. The main results of our analysis are: (i) The VB's and CB of bulk constituents are highly non-parabolic and anisotropic. At the energy range of 45–80 meV from bandedge, we observe strong non-parabolicity in the CB and light hole VB of bulk materials at the Γ point. If a model of bandstructure is used which does not capture full bandstructure details of the bulk materials the superlattice bandstructure obtained from such a model will not be reliable. (ii) The bandstructure we have used to model the superlattices fits the effective masses at the Γ and X points in the Brillion zone. It is critical to have a good effective mass fit in order to evaluate the DOS accurately. (iii) An accurate calculation of DOS is done. (iv) We have calculated the impact of the InSb monolayer on the electron and hole distributions in the superlattice unit cell. The overlap of the wavefunctions determines the optical properties of the detector. (v) We have calculated the variation of E_g with layer thicknesses of the constituents. We observe that introducing the InSb monolayer (used for strain compensation) lowers the E_g of the structure. (vi) A calculation of carrier concentration or doping as a function of position of E_F has been done. This calculation can be used to represent the InAs-InSb/GaSb type-II superlattice as an effective material in further transport calculations.

Hence, we conclude that a full bandstructure representation of InAs-InSb/GaSb type-II SL is required to accurately analyze carrier transport in the devices fabricated using these SL.

ACKNOWLEDGMENTS

We acknowledge helpful discussions with William Vandenberghe in the final stages of completion of this manuscript.

[1] D. L. Smith and C. Mailhiot, J. Appl. Phys. **62**, 2545 (1987).
[2] D. Z.-Y. Ting, A. Soibel, C. J. Hill, J. Nguyen, S. A. Keo, S. B. Rafol, B. Yang, M. C. Lee, J. M. Mumolo, J. K. Liu, *et al.*, Infrared Phys. Technol. **54**, 267 (2011).
[3] P. Klipstein, O. Klin, S. Grossman, N. Snapi, I. Lukomsky, M. Yassen, D. Aronov, E. Berkowitz, A. Glozman, O. Magen, I. Shtrichman, R. Frenkel, and E. Weiss, Proc. SPIE **8268**, 82680U (2012).
[4] C. H. Grein, M. E. Flatte, J. T. Olesberg, S. A. Anson, L. Zhang, and T. F. Boggess, J. Appl. Phys. **92**, 7311 (2002).
[5] Y. Wei and M. Razeghi, Phys. Rev. B **69**, 085316 (2004).
[6] X.-L. Lang and J.-B. Xia, J. Phys. D **44**, 425103 (2011).
[7] F. Szmulowicz, H. Haugan, and G. Brown, Phys. Rev. B **69**, 155321 (2004).
[8] J. H. Davies, *The Physics of Low-Dimensional Semiconductors: An Introduction* (Cambridge University Press, 2005).
[9] J. C. Slater and G. F. Koster, Phys. Rev. **94**, 1498 (1954).
[10] P. Vogl, H. P. Hjalmarson, and J. D. Dow, J. Phys. Chem. Solids **44**, 365 (1983).
[11] T. B. Boykin, J. James, and S. Harris, J. Appl. Phys. **72**, 988 (1992).
[12] F. Oyafuso, G. Klimeck, R. C. Bowen, T. Boykin, and P. von Allmen, Phys. Status Solidi C **0**, 1149 (2003).
[13] T. Xia, L. Register, and S. K. Banerjee, IEEE Trans. Electron Devices **50**, 1511 (2003).
[14] A. Pecchia and A. D. Carlo, Rep. Prog. Phys. **67**, 1497 (2004).
[15] H. Minari and N. Mori, J. Comput. Electron. **6**, 223 (2007).
[16] M. Usman, H. Ryu, I. Woo, D. Ebert, and G. Klimeck, IEEE Trans. Nanotechnol. **8**, 330 (2009).
[17] T. Boykin, M. Luisier, N. Kharche, X. Jaing, S. Nayak, A. Martini, and G. Klimeck, in *Computational Electronics (IWCE), 2012 15th International Workshop on* (2012), pp. 1–4.
[18] T. B. Boykin, Phys. Rev. B **54**, 8107 (1996).
[19] P. Pinsukanjana, private communication (2012).
[20] T. B. Boykin, Phys. Rev. B **56**, 9613 (1997).
[21] H. Kroemer, Physica E **20**, 196 (2004).
[22] R. Chen and C. Persson, J. Appl. Phys. **112**, 103708 (2012).
[23] B. Klein, E. Plis, M. N. Kutty, N. Gautam, A. Albrecht, S. Myers, and S. Krishna, J. Phys. D **44**, 075102 (2011).
[24] B. K. Ridley, *Quantum Processes in Semiconductors* (Oxford Science Publications, 1982).